Article

Lattice Matched Carbide-Phosphide Heterostructures with Superior Electrocatalytic Activity and Stability

Yagya N. Regmi, Asa Roy, Laurie A. King, David A. Cullen, Harry M. Meyer, Gabriel A. Goenaga, Thomas A. Zawodzinski, Nicole Labbe, and Stephen C. Chmely

Chem. Mater., **Just Accepted Manuscript** • DOI: 10.1021/acs.chemmater.7b03377 • Publication Date (Web): 19 Oct 2017

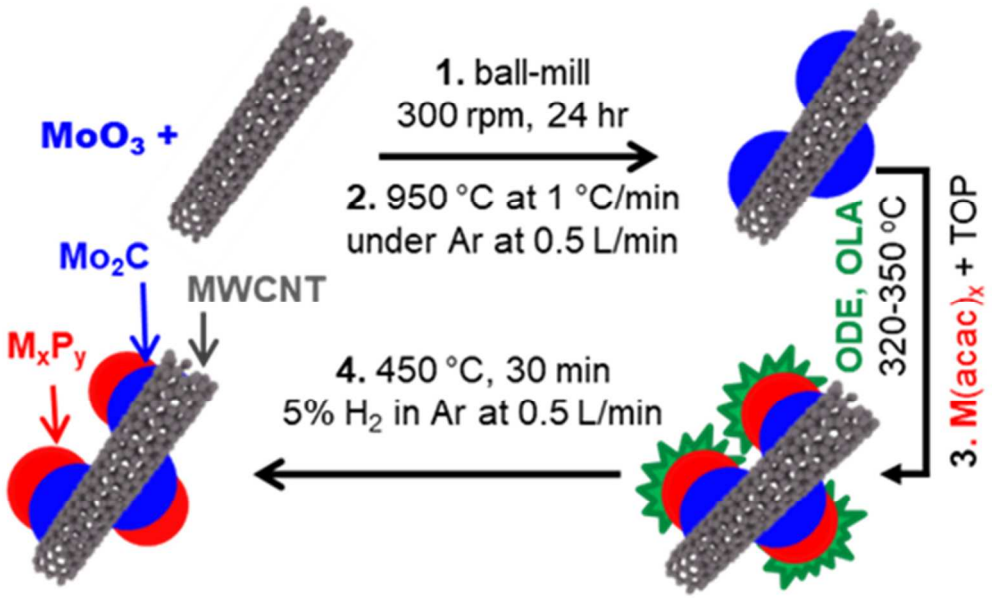

Sequential synthesis method for carbide-phosphide composites.

84x50mm (300 x 300 DPI)

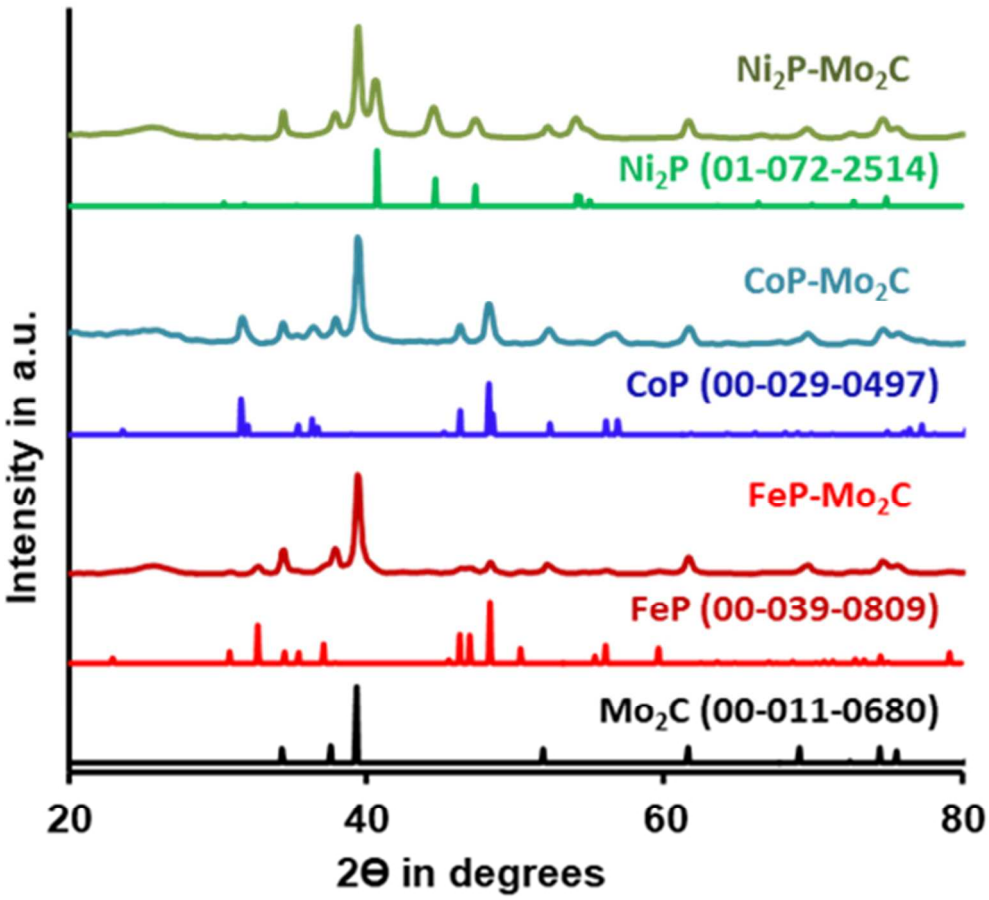

Figure 1. PXRD patterns of metal phosphide (MP) deposited carbide composites (MP-Mo2C) and the corresponding reference patterns with the PDF numbers.

84x77mm (300 x 300 DPI)

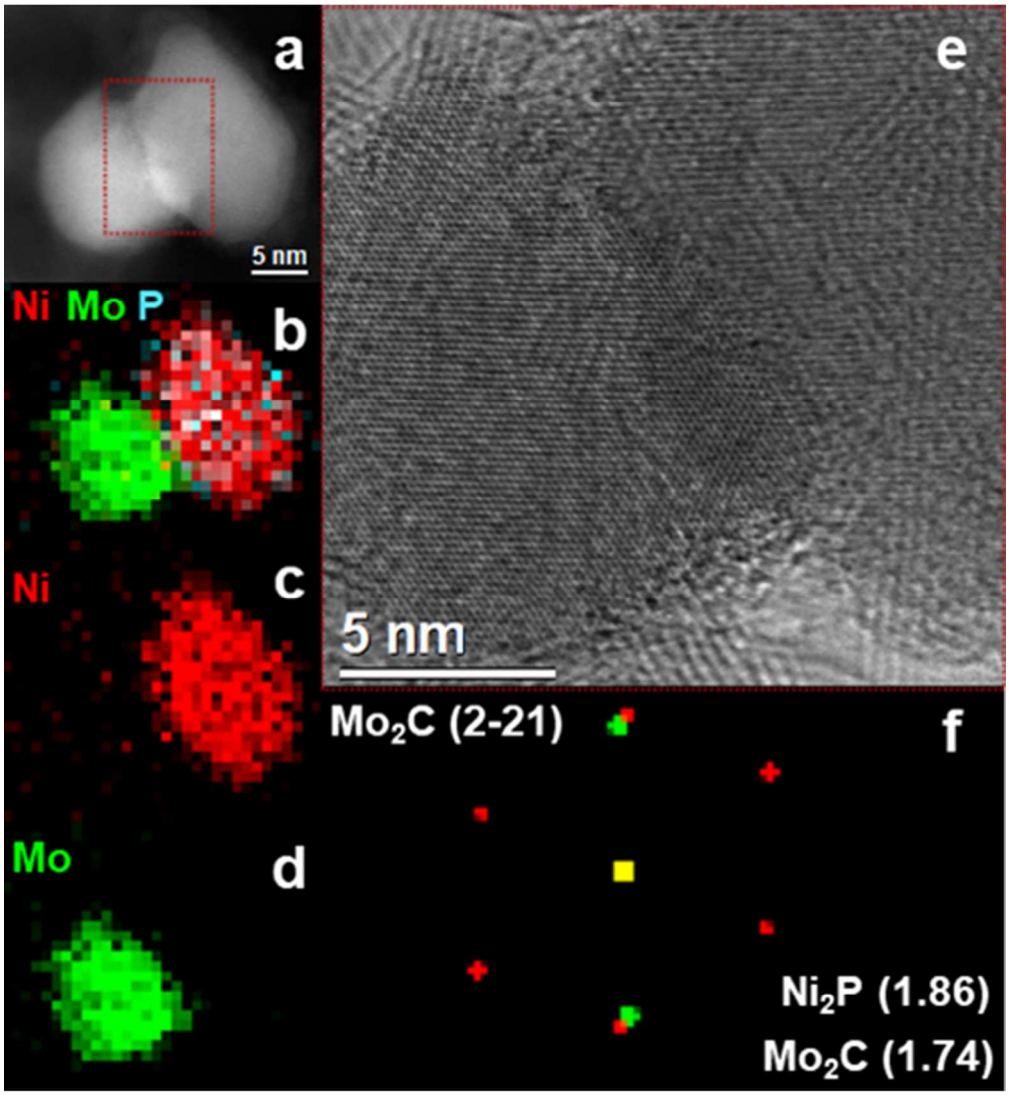

Figure 2. (a) High-angle annular dark-field scanning transmission electron microscopy (HAADF-STEM) image of a Ni2P-Mo2C particle. (b) Electron energy loss spectroscopy (EELS) spectrum image with Ni (red), P (blue) and Mo (green). (c) Mo M-edge and (d) Ni L–edge EELS maps. (e) HRTEM image centered along the interface, and (f) fast Fourier transform (FFT) with Mo2C(2-21) zone axis and measured Ni2P and Mo2C lattice spacing indicated.

84x91mm (300 x 300 DPI)

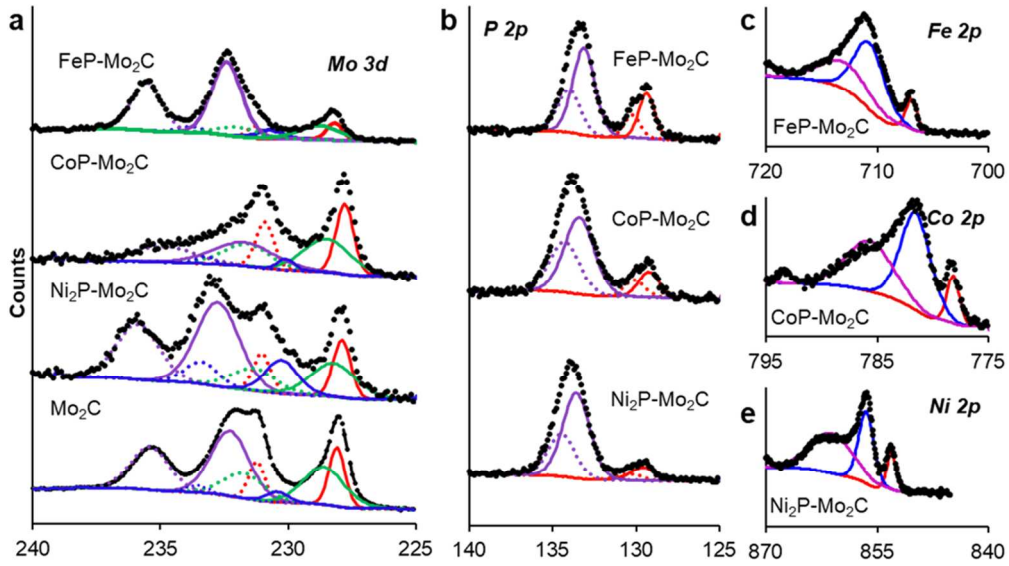

Figure 3. (a) High resolution XPS Mo 3d plots of carbide-phosphide composites and Mo2C. (b) P 2p and (c-e) metal 2p plots corresponding to Mo2C deposited with phosphide. Solid fitting lines represent curves for 3d5/2 in Mo 3d and 2p3/2 in P 2p plots. The dashed color coded lines are corresponding 3d3/2 and 2p1/2 curves, respectively.

177x101mm (300 x 300 DPI)

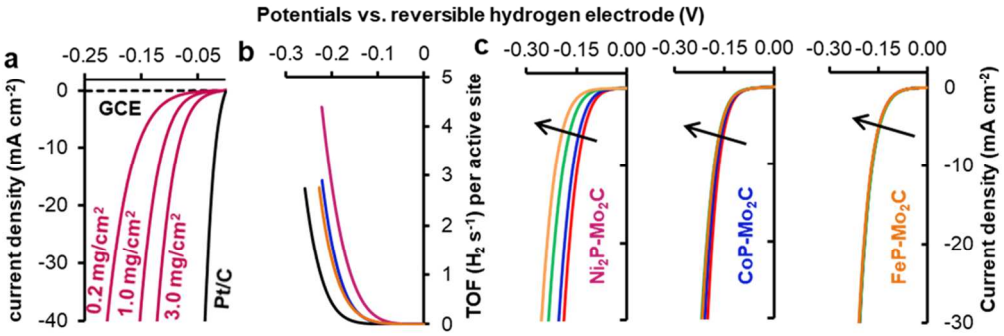

Figure 4. (a) HER polarization curves for Ni2P-Mo2C catalyst in 0.5 M H2SO4. GCE is bare glassy carbon electrode and Pt/C is 30 weight % Pt on carbon. (b) Turn over frequency (TOF) plots of Mo2C (black); and FeP (orange), CoP (blue) and Ni2P (purple) loaded CPCs at 0.2 mg cm-2. (c) HER polarization curves for the composite catalysts collected after 0 hr (red), 6 hr (blue), 12 hour (green), 18 hr (orange) of constant potential electrolysis (CPE) at applied iR corrected potentials corresponding to 10 mA cm-2.

177x60mm (300 x 300 DPI)

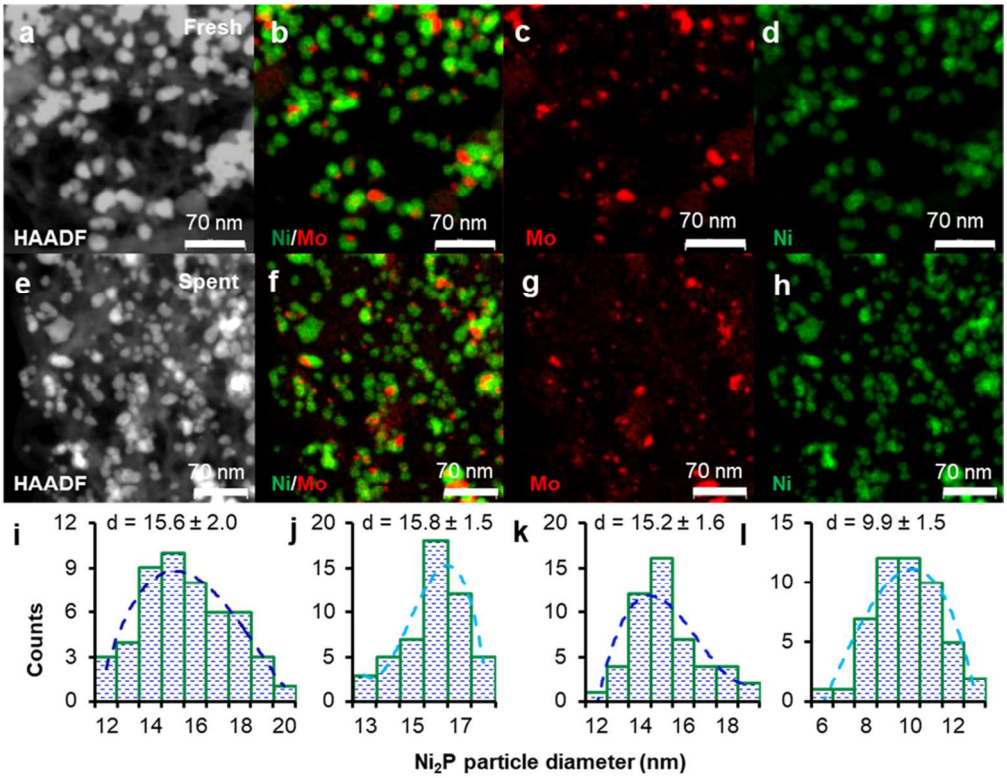

Figure 5. HAADF image and EDS maps of fresh (a-d) and spent (e-h) Ni2P-Mo2C. Nickel (green) and molybdenum (red) are overlaid in b and f. Particle size distribution of Ni2P in the composite catalyst corresponding to i) fresh catalyst with Ni2P deposited on Mo2C j) fresh catalyst with Ni2P not directly deposited on Mo2C k) spent catalyst with Ni2P deposited on Mo2C and l) spent catalyst with Ni2P not directly deposited on Mo2C. Direct deposition implies overlap of Mo and Ni in EDS maps.

177x137mm (300 x 300 DPI)

Lattice Matched Carbide-Phosphide Composites with Superior Electrocatalytic Activity and Stability

Yagya N. Regmi[¤,*], Asa Roy[‡,#], Laurie A. King[§], David. A. Cullen[¶], Harry M. Meyer III[¶], Gabriel A. Goenaga[†], Thomas A. Zawodzinski Jr[†,‡,#], Nicole Labbé[¤], and Stephen C. Chmely[¤,*]

[¤]Center for Renewable Carbon, University of Tennessee, Knoxville, TN, 37996, USA.

[†]Department of Chemical and Biomolecular Engineering, University of Tennessee, Knoxville, TN, 37996, USA.

[§]Department of Chemical Engineering, Stanford University, Stanford, CA, 94305, USA.

[¶]Materials Science and Technology Division, Oak Ridge National Laboratory, Oak Ridge, TN, 37831, USA.

[‡]Oak Ridge National Laboratory, Oak Ridge, TN, 37831, USA.

[#]Bredesen Center for Interdisciplinary Research and Education, Knoxville, TN, 37996, USA.

Carbide, phosphide, electrocatalysis, hydrogen evolution reaction, composite materials

ABSTRACT: Composites of electrocatalytically active transition metal compounds present an intriguing opportunity towards enhanced activity and stability. To identify potentially scalable pairs of catalytically active family of compounds, we demonstrate that phosphides of iron, nickel, and cobalt can be deposited on molybdenum carbide to generate nanocrystalline heterostructures. Composites synthesized via solvothermal decomposition of metal acetylacetonate salts in the presence of highly dispersed carbide nanoparticles show comparable hydrogen evolution activities to the state-of-the-art non-noble metal catalysts. Investigation of the spent catalyst using high resolution microscopy and elemental analysis reveals that formation of carbide-phosphide composite prevents catalyst dissolution in acid electrolyte. Lattice mismatch between the two constituent electrocatalysts can be used to rationally improve electrochemical stability. Among the composites of iron, nickel, and cobalt phosphide, iron phosphide displays the lowest degree of lattice mismatch with molybdenum carbide and shows optimal electrochemical stability. Turnover rates of the composites are higher than the carbide substrate and compare favorably to other electrocatalysts based on earth-abundant elements. Our findings will inspire further investigation into composite nanocrystalline electrocatalysts that implement molybdenum carbide as a stable catalyst support.

1. INTRODUCTION

A critical technological challenge is the production and storage of renewable energy to meet the demands of the global population. Electrochemical water splitting is one of the most promising energy conversion routes towards renewable energy storage in the chemical bonds of hydrogen.[1] To date, platinum deposited on carbon (Pt/C) has the optimal catalytic activity towards the hydrogen evolution reaction (HER).[2] The limited earth abundance of such precious metals, however, lowers the economic and environmental sustainability of hydrogen generated using these materials. Thus, there has been significant investment in recent years towards the identification of materials based on earth-abundant metals that can approach the activity and stability of Pt/C for HER.[3-6] HER using earth-abundant transition metal (TM) catalysts has been demonstrated to be almost comparable to Pt/C, albeit only when activity is normalized to geometric surface area of the working electrode.[7] Pt/C outperforms all reported TM catalysts when activity is normalized to the electrochemical active surface area (ECSA).[8]

Molybdenum carbide is one of the most active and stable HER electrocatalysts among transition metal carbides (TMC).[9-11] Although various routes have been developed for carbide synthesis, temperature programmed reduction, using an explosive mixture of H_2 and CH_4 gases, has thus far been the preferred method for preparing Mo_2C catalysts.[12] A more benign and reproducible carbothermic reduction synthesis, using inert Ar as the only flow gas, has also been developed and shown to prepare active, stable, and scalable Mo_2C electrocatalysts.[13] In addition, nanostructured transition metal phosphides (TMP) of Fe, Ni, Co and Mo have been prepared from the solvothermal decomposition of inorganic and organometallic precursors in the presence of trioctylphosphine (TOP). HER active TMP electrocatalysts have been shown to possess some of the highest activities reported for materials based on earth-abundant metals.[14-16] In order to prevent agglomeration during annealing and electrocatalysis, TMP

nanoparticles have been immobilized either on metal foils or decorated on high surface area carbon structures.[17-20]

Highly structured carbon and conductive Ti foils are reasonably stable and inexpensive substrates for catalysts, but catalytically active substrates provide an intriguing alternative towards preparing advanced composites. Such catalytically active substrates can either enhance the overall mass activity of the material, or more importantly, can be used to integrate multiple catalytic processes in one complete system. Nanoreactors have been prepared that combine solar energy harvesting with electrochemical water splitting via a composite of an electrocatalyst and a semiconductor.[21-23] Similarly, one could envision using in-situ generated H_2 to initiate hydrodeoxygenation (HDO) species by immobilizing a HDO catalyst on HER active substrates. However, there remain significant challenges to such a strategy, including identification of compatible material pairs, feasibility of scaled up synthesis, and stability of the integrated reactors.[24-28] Still, composite materials that can enhance or combine catalytic activities into a single integrated particle are highly desirable.

Herein, we investigate the deposition of transition metal phosphide nanoparticles onto Mo_2C nanoparticles via solvothermal decomposition. We prepare Mo_2C nanoparticles using a simple and scalable carbothermic reduction method. Our motivation for this material combination is to exploit potential lattice matching, which we reveal by aberration-corrected high-resolution scanning transmission electron microscopy (HRSTEM), electron energy loss spectroscopy (EELS), X-ray photoelectron spectroscopy (XPS), and powder X-ray diffraction (PXRD). Then, we employ the carbide-phosphide composites (CPC) of FeP, CoP, and Ni_2P on Mo_2C as catalysts for HER in 0.5 M H_2SO_4 using a three electrode rotating disc (RDE) setup. We investigate electrochemical stabilities under HER conditions. We examine spent catalyst using HRSTEM, energy dispersive X-ray spectroscopy (EDS) and analyze spent electrolyte using inductively-coupled plasma optical-emission spectroscopy (ICP-OES). We also compare the HER activities with other non-precious-metal catalysts with respect to their intrinsic catalytic properties and active site loading. In addition, we estimate catalytic efficiency by calculating turn over frequency (TOF) for HER. Finally, we investigate the degradation behavior of the composite catalysts under electrochemical conditions.

2. EXPERIMENTAL SECTION

2.1 Materials. MoO_3, 70-80 % C multiwalled carbon nanotubes (MWCNT), oleylamine (OLA), 5 % Nafion® (IonPower), and methanol were purchased from Sigma-Aldrich. $Ni(acac)_2$, $Co(acac)_2$ and $Fe(acac)_3$, TOP, 1-octadecen (ODE) were purchased from Across Organics. Hexanes (a mixture of structural isomers) and anhydrous ethanol were obtained from Fisher Scientific. 99.999 % H_2SO_4 was purchased from Alfa Aesar. Pt/C (30 weight % on Vulcan XC-72) catalyst was purchased from Tanka. Ultra-pure nitrogen, 5 % H_2 in Ar and Ar were procured from Airgas. ICP-OES standards for Mo, Ni, Co, Fe and P were obtained from SPEX CertiPrep.

2.2 Carbide synthesis. Mo_2C templated on MWCNT was synthesized using a recently reported ball-milling and carbothermic reduction method.[29] In brief, a 20:1 mass ratio of ball to a mixture of MoO_3 and MWCNT was ball-milled for 20 hours at 300 rpm followed by carbothermic reduction under Ar atmosphere at 950 ºC. The ramping rate was 1 ºC min^{-1}, the Ar flow rate was 0.5 L min^{-1}, and the tube furnace was allowed to cool naturally to ambient temperature without any dwell time at 950 ºC. The nanocrystalline powder was then ground to a fine powder using an agate mortar and pestle.

2.3 Phosphide and CPC synthesis. Ni_2P and Ni_2P-Mo_2C were synthesized using a direct solvothermal decomposition method reported by Popczun et al.[18] In brief, 0.250 g (0.98 mmol) $Ni(acac)_2$, 4.5 mL (14.1 mmol) ODE, 6.4 mL (19.5 mmol) OLA and 2 mL (4.4 mmol) TOP were added to a three-neck round bottom flask equipped with a thermometer to monitor temperature, condenser, and magnetic stir bar. The flask was then refluxed at 120 ºC for 60 minutes under vacuum while continuously stirred at 300 rpm. The flask was then filled with N_2 and refluxed at 320 ºC for 120 minutes. The heating mantle was turned off, which allowed the mixture to cool to 200 ºC. Then, the hot mantle was subsequently removed from under the flask to initiate rapid cooling to ambient temperature. The nanoparticles were separated from the synthesis mixture by centrifugation at 4000 x g and were subsequently washed with 3 portions of a mixture composed of 1:3 (v:v) hexane:ethanol. The product nanocrystals were then re-suspended in hexane for storage. The synthesis of Ni_2P-Mo_2C was analogous, except for the addition of 0.1320 g of Mo_2C. Desired mass of nanocrystalline powders were separated from hexane via centrifugations and annealed in a quartz boat at 450 ºC for 60 minutes to remove organic adsorbates. The ramp rate was 10 ºC min^{-1}, and 5% H_2 in Ar was the flow gas at 0.5 L min^{-1}. The annealed catalysts were ground to a fine powder using an agate mortar and pestle prior to characterization and catalysis. Synthesis and post-synthesis preparation for CoP and CoP-Mo_2C was analogous to Ni_2P and Ni_2P-Mo_2C, respectively, with slight modifications in precursor ratios and decomposition temperature elevated to 330 ºC. A mixture of 0.500 g (1.94 mmol) $Co(acac)_2$, 9 mL (14.1 mmol) ODE, 12.8 mL (19.5 mmol) OLA and 8.8 mL (19.4 mmol) TOP constituted the precursor mixture for CoP and 0.2640 g of Mo_2C was added to the precursor mixture for the synthesis of CoP-Mo_2C. The phosphide and composite synthesis and preparations for iron were analogous to that of Co and CoP-Mo_2C systems except for the decomposition temperature of 350 ºC. 0.6851 g $Fe(acac)_3$ was added to afford 1.94 mmol of iron precursor in the mixture.

2.4 Control catalyst synthesis. TMP deposited on MWCNT (TMP-MW) were prepared by substituting carbide with MWCNT in the precursor mixture for solvothermal decomposition. Synthesis and work up of the physical mixture of TMP and Mo_2C (TMPmixMo_2C) was analogous to CPC except the decomposition of acac pre-

cursor was carried out in the absence of carbide. Instead, as-synthesized carbide and phosphide nanoparticles were mixed via sonication and centrifugation prior to annealing. Please see supporting information for additional details.

2.5 Physical characterization. A Pananalytical Empyrean diffractometer with Cu K-alpha 1 source (λ = 1.5406 Å) was for PXRD. Background from instrumental broadening for Scherrer analysis was based upon LaB_6 standard (660) purchased from the National Institute of Standards and Technology (NIST). The reference patterns were obtained from PDF-4 database from International Center for Diffraction Data (ICDD).

XPS were collected on a Thermo Scientific Model K-Alpha instrument. The source was monochromated, micro-focusing, Al Kα X-ray (1486.6 eV). A 400 μm X-ray spot size was used to maximize signal and average surface area composition. The detector was a 128 multi-channel hemispherical electron energy analyzer. The analysis chamber pressure was maintained at or below 2 x 10^{-9} mbar, and was lowered to 2 x 10^{-7} when the flood gun was operating. Samples were prepared by dispersing a small amount of powder on double-sided tape. Enough powder was used to completely obscure the tape. Analyzer pass energy was 200 eV for survey spectra and 50 eV for specific elemental analysis. Charging was avoided by optimizing charge compensation via a combination of low energy electrons and low energy argon ions. Initial data analysis was performed using the Avantage XPS software package (v 4.61) while the high resolution XPS peak deconvolution was performed using CasaXPS software (v 2.3.16).

ICP-OES measurements were performed on an Optima 7300 DV spectrometer from PerkinElmer with as obtained electrolyte diluted (x10) with carrier solvent, 1.12 M (5 %, w/w) nitric acid.

Scanning electron microscopy (SEM) images were collected on a Zeiss EVO instrument equipped with an EDS detector from Bruker. SEM samples were deposited on double sided carbon tape for analysis. TEM samples were prepared by sonicating the powders in isopropanol then dropcasting the solution on Cu-supported lacey-carbon grids. Electron microscopy characterization was performed on a Nion UtraSTEM U100 operated at 100kV and equipped with a Gatan Enfina electron energy loss spectrometer.

2.6 Electrochemical characterization. Electrochemical analysis was performed on a Pine Instrument RDE and VMP-3 potentiostat from BioLogic Science Instruments. 5 mm diameter glassy carbon electrode (GCE) was the working electrode and a gold wire as the counter electrode. The reference was a Radiometer Analytical XR-200 $Hg/HgSO_4$ electrode. All potentials were adjusted to RHE and the potential of the reference electrode was determined by measuring the open circuit voltage of a Pt electrode in hydrogen saturated electrolyte.[29] Catalyst inks were prepared by adding 2.6 mg of catalyst to 0.5 ml of methanol and 38 μL of Nafion and sonicated for 20 minutes. The required volume for the 200 μg cm^{-2} was determined by depositing aliquots of the inks onto Al foil and weighing with a Mettler Toledo XP2U balance. GCE working electrodes were prepared by polishing sequentially with 5.0 micron and 0.05 micron alumina powders, rinsing and sonicating in ultrapure water for 5 minutes followed by sonicated in 0.5 M H_2SO_4 for 5 minutes. The electrodes were also cleaned electrochemically by scanning 10 cyclic voltammetry (CV) scans at 50 mV/s between 0.1 and -0.8 V in N_2 saturated electrolyte. The background activity of the clean GCE was measured by collecting CVs between 0.1 and -0.8 V at a scan rate of 5 mV s^{-1} in H_2 saturated electrolyte. Working electrodes were rotated at 3500 rpm to remove in-situ generated gas bubbles. Afterward, the predetermined volume of catalyst ink was deposited onto the electrode. Electrolytes were saturated with H_2 throughout HER. The catalyst surface was first electrochemically cleaned in a similar manner to the bare GCE with the potential window selected to limit the current to 50 mA cm^{-2}. After cleaning, the activities were measured by collecting 5 CVs within the same potential window at a 5 mV s^{-1} scan rate followed by 5 HER polarization curves. Potentio electrochemical impedance spectroscopy measurements were conducted at 0 V for each electrode in order to iR correct the data. The ECSA of catalysts was determined by measurement of the double-layer capacitance described in detail in a recent report.[29] These measurements were made by collecting CVs within the range 0-0.3 V at 100, 50, 20, 10, and 5 mV s^{-1} scan rates. The fifth cycle was collected for the first three scan rates and the third cycle for the latter two in order to ensure stable values were selected. For most catalysts, no faradaic processes were observed within these regions. The Tafel slopes of each polarization curves were determined around the onset potentials according to the method described previously.[13] The stability experiments were conducted for the catalysts by holding the electrode at the overpotential corresponding with a 10mA cm^{-2} current density. A graphite rod was used as the counter electrode for the long term stability tests. After 6 hour, 5 polarization curves were collected at 5mV s^{-1} scan rate. This process was repeated after each additional 6 hours.

3. RESULTS AND DISCUSSION

3.1 Catalyst synthesis. A modified sequential synthesis method used to prepapre hydrothermally synthesized Ni_2P-Mo_2C composites and illustrated in Scheme 1 was employed to prepare the composites.[30] Phosphides were synthesized via direct decomposition of their respective acetylacetonate (acac) salts in ODE.[31-33] We employed TOP as both the source of phosphorus and as a stabilizing ligands and OLA as the reducing agent. Mo_2C decorated on MWCNT was separately prepared using a carbothermic reduction method.[34] We have modified the phosphide synthesis to prepare new carbide-phosphide composites by adding Mo_2C to the phosphide synthesis precursor. Carbothermic reduction derived Mo_2C contains about 40 % by weight of carbide and the rest of the matrix is unreacted carbon.[13] More descriptive nomenclature for carbide and composites would be Mo_2C-MWCNT and

TMP-Mo_2C-MWCNT, respectively. However, for efficiency, we hereafter refer to the materials as Mo_2C and TMP-Mo_2C, respectively. Recently, we reported a hydrothermal method to prepare composites of Ni_2P and Mo_2C.[29] To the best of our knowledge, this is the first report on solvothermal decomposition derived synthesis of TMP on Mo_2C. It is also the first report on synthesis and characterization of the composites of FeP and CoP with Mo_2C using any synthesis route.

Scheme 1. Sequential synthesis method for carbide-phosphide composites.

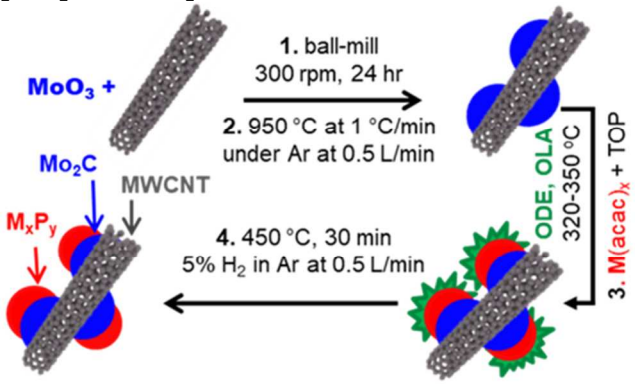

Among nickel phosphides, Ni_2P nanoparticles synthesized using the acac decomposition method show monodispersity centered around 21 nm.[18] Mo_2C substrate crystallites are also about 21 nm on average, thus facilitating EELS investigations. FeP and CoP were selected because they have shown enhanced activity towards HER electrocatalysis in comparison to other iron and cobalt phosphide phases.[35, 16] Nanocrystalline Ni_2P formed at 320 ºC, but the temperatures for CoP and FeP synthesis had to be elevated to 330 ºC and 350 ºC, respectively. The resultant nanocrystals of Ni_2P remained suspended in hexane for days until centrifuged for annealing, but the CoP and FeP nanocrystals separated within minutes. All nanocrystalline composites also precipitated in hexane within minutes.

3.2 Physical characterization. The PXRD patterns of the synthesized phosphide-carbide composites are shown in Figure 1. These data indicate the successful synthesis of monophasic phosphides on Mo_2C. All the peaks in the diffractograms for the composite materials can be assigned to either the phosphide or Mo_2C. This is an indication that the crystal structure of the carbide remains unchanged during the solvothermal synthesis and the subsequent annealing step. The broad peaks around 25° in the composite diffractograms correspond to graphitic carbon from MWCNT, further emphasizing the presence of ubiquitous amount of unreacted carbon in carbide matrix.[36] Scherrer analysis of the diffraction peaks reveals the Mo_2C and Ni_2P crystallites to be approximately 19 nm and 17 nm, respectively. Similarly, the crystallite size for FeP and CoP are estimated to be approximately 19 and 23 nm, respectively. Since the phosphide crystallite sizes are fairly similar, we infer that rapid precipitation of CoP and FeP in hexane is probably due to the formation of clusters.

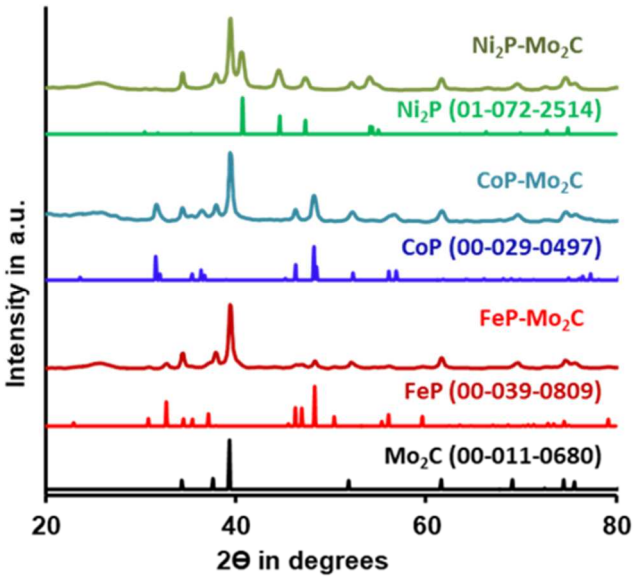

Figure 1. PXRD patterns of metal phosphide (MP) deposited carbide composites (MP-Mo2C) and the corresponding reference patterns with the PDF numbers.

When the synthesis was carried out in the absence of Mo_2C, biphasic phosphides were obtained (Figure S1). Recent investigations to synthesize composites of Ni_2P and Mo_2C using a hydrothermal synthesis method also demonstrated that carbide-phosphide interaction is crucial to maintain monophasic phosphide.[30] Other investigations of supported phosphides have employed a conductive substrate such as carbon cloth, carbon fibers, and nickel foams to maintain monophasic material.[37-39] Here, we initially employed no support for phosphides to highlight the importance of immobilizing the catalyst on a conductive surface to prevent aggregation and phase inhomogeneity during annealing. Similar to CPCs in Figure 1, when MWCNT is used as the phosphide support the resulting TMP-MW composites also reveal monophasic phosphides (Figure S2).

The HAADF-STEM micrograph in Figure 2a and EELS elemental maps of a composite Ni_2P-Mo_2C nanoparticle in Figure 2b-d show that the constituent materials maintain their nanostructures (~ 20 nm) post-annealing. The lattice planes forming the interfacial region shown in Figure 2e can be identified by analysis of the fast Fourier transform (FFT) in Figure 2f. Interfacial structural information is particularly beneficial because it provides insight into the nature of bimetallic active sites that may arise via interaction between the two materials. Attempts to employ EELS studies were limited to Ni_2P-Mo_2C because CoP-Mo_2C and FeP-Mo_2C composites form significantly bigger clusters, perhaps due to the higher temperatures necessary during synthesis.

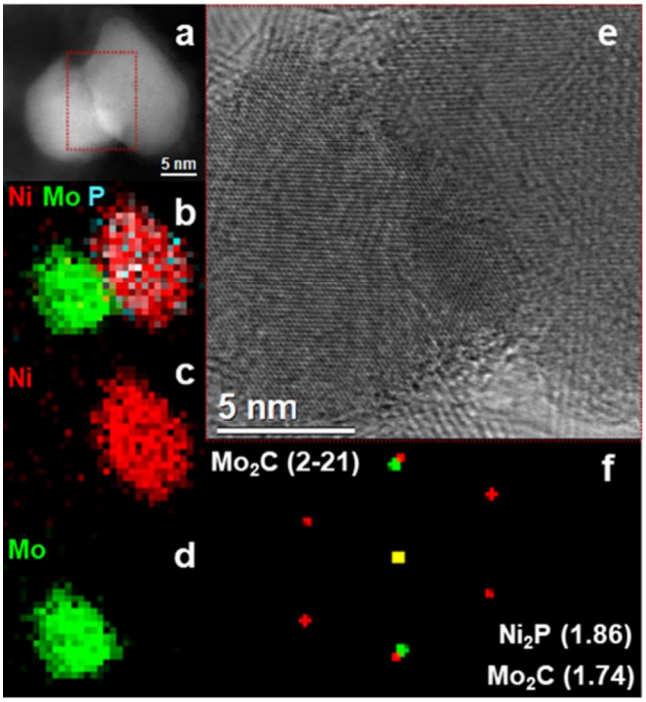

Figure 2. (a) High-angle annular dark-field scanning transmission electron microscopy (HAADF-STEM) image of a Ni_2P-Mo_2C particle. (b) Electron energy loss spectroscopy (EELS) spectrum image with Ni (red), P (blue) and Mo (green). (c) Mo M-edge and (d) Ni L–edge EELS maps. (e) HRTEM image centered along the interface, and (f) fast Fourier transform (FFT) with Mo_2C(2-21) zone axis and measured Ni_2P and Mo_2C lattice spacing indicated.

XP survey spectra of as synthesized catalysts (Figure S3) indicate that the composite surfaces are more oxidized than Mo_2C surface. O accounts for 9 % of the carbide surface, but the contribution from O ranges from 14 to 21 % for the composites (Table S1). High resolution XPS spectra of composites and Mo_2C surfaces (Figure 3) show that the distributions of Mo sites on the composite surfaces are similar to previous investigations on Fe, Co, or Ni-doped Mo_2C (Table S2).[40-42] The metals in the phosphides are evidently interacting with Mo in carbide.

Phosphorus 2p spectra in Figure 3b indicates presence of phosphide (129 eV) as well as oxidized (133 eV) phosphorus species.[43] Metal 2p spectra in Figure 3c-e further corroborate the presence of metal phosphide (778 eV for Co, 707 eV for Fe and 853 eV for Ni) in addition to metal oxide bonds at higher binding energies.[44-47] Presence of metal oxides and oxidized phosphorus species on the catalyst surfaces is typical of metal phosphide nanomaterials and has been discussed in detail previously.[15]

In a recent report, Shi et al. reported that P doping into Mo_2C (P-Mo_2C) leads to superior electrocatalytic activities.[48] Amorphous MoP is also a good electrocatalyst.[49] PXRD plots in Figure 1 indicate the absence of crystalline MoP. The synthesis and annealing temperatures employed here (≤450 °C) are lower than those in P-Mo_2C (900 °C). Formation of amorphous MoP would lower the binding energy (B.E.) of Mo^{2+} peaks across the three composites relative to Mo_2C, as observed for P-Mo_2C.[48] The inconsistent B.E. for Mo $3d_{5/2}$ peaks (Table S2) and the overall Mo 3d spectra in Figure 3a are more akin to Mo_2C

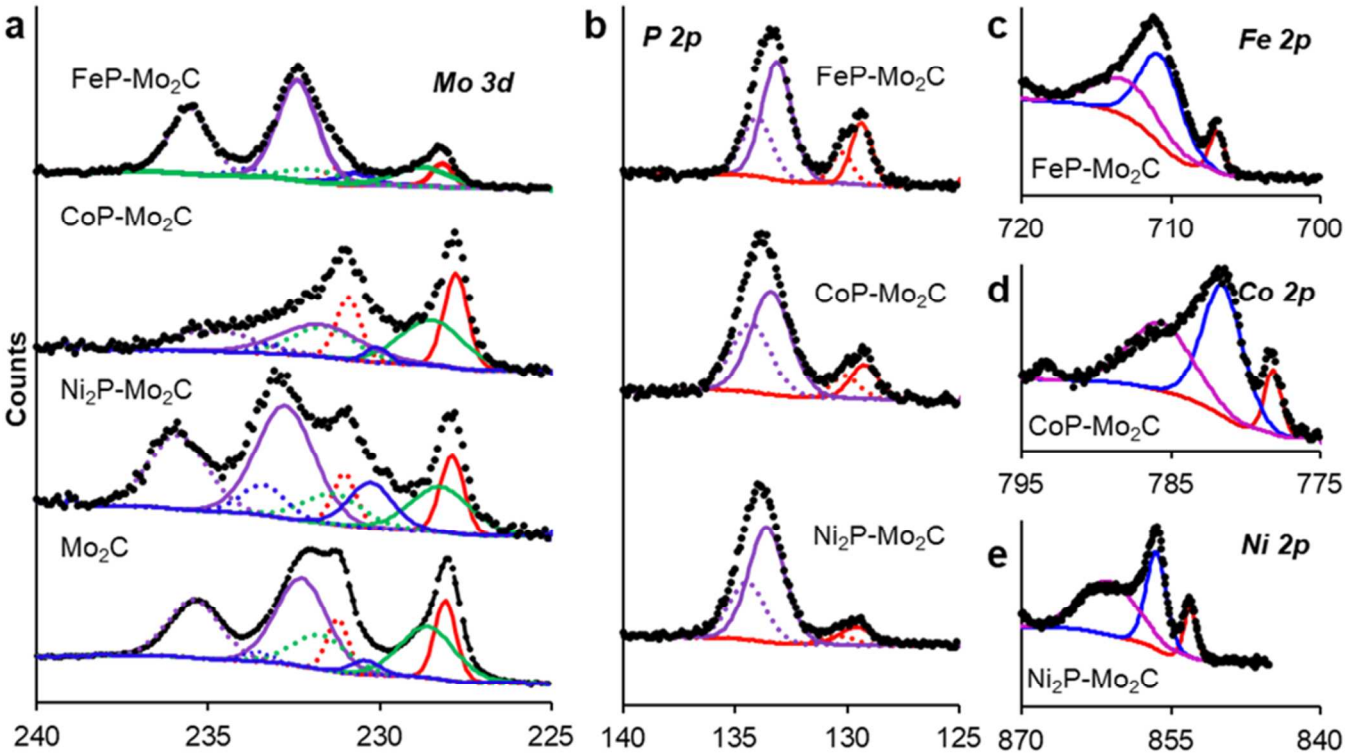

Figure 3. (a) High resolution XPS Mo 3d plots of carbide-phosphide composites and Mo_2C. (b) P 2p and (c-e) metal 2p plots corresponding to Mo_2C deposited with phosphide. Solid fitting lines represent curves for $3d_{5/2}$ in Mo 3d and $2p_{3/2}$ in P 2p plots. The dashed color coded lines are corresponding $3d_{3/2}$ and $2p_{1/2}$ curves, respectively.

doped with Fe, Ni, and Co rather than P-Mo_2C, further indicating the absence of any Mo-P bond formations. Thus, it can be inferred that amorphous MoP is also unlikely to be present.

3.3 Catalysis. HER activities of unsupported phosphides, unadulterated Mo_2C, and CPCs were collected in acid electrolyte and are presented in Table 1. The overpotentials, ECSA, and Tafel slopes are an average of at least five independent measurements (Table S3). Several factors, including electrochemical environment, catalyst loading, adjustments for internal resistance, and area used for activity normalization need to be carefully considered for accurate comparison of the catalytic activities of nanostructured materials.[7, 50, 51] CPCs show substantial reduction in overpotential when compared to unadulterated Mo_2C. These numbers are comparable to other phosphide catalysts assessed under analogous electrochemical conditions and catalyst loadings (0.2 mg cm^{-2}).[16] Actual phosphide loading is around 0.1 mg cm^{-2} because the phosphide-to-carbide molar ratio is maintained at 2:1.[29]

Table 1. HER overpotentials (iR corrected) for 10 mA/cm^2 activity, ECSA and Tafel slopes in 0.5 M H_2SO_4. The statistical errors are indicated in parenthesis.

	$\eta_{10\ mA\ cm^{-2}}$ (mV)	ECSA (cm^2)	Tafel slope (mV/dec)
Ni_2P-Mo_2C	154 (1)	22 (1)	83 (<1)
CoP- Mo_2C	158 (1)	34 (1)	56 (<1)
FeP-Mo_2C	169 (1)	29 (2)	62 (<1)
Ni_2PmixMo_2C	195 (2)	51 (6)	69 (6)
CoPmixMo_2C	192 (8)	47 (4)	54 (4)
FePmixMo_2C	202 (2)	46 (11)	58 (2)
Ni_2P-MW	243 (9)	15 (6)	72 (7)
CoP-MW	196 (6)	14 (5)	50 (1)
FeP-MW	195 (9)	11 (5)	72 (4)
Ni_2P	603 (49)	<1	202 (24)
CoP	426 (15)	<1	103 (9)
FeP	286 (21)	4 (1)	78 (4)
P-MW	387 (11)	8 (5)	112 (8)
Mo_2C	206 (1)	31 (2)	59 (3)

The HER overpotentials for TMP-MW and physical mixtures in Table 1 are lower than unsupported phosphides but they are higher than corresponding CPCs. Comparison of the ECSA and overpotentials of CPCs with physical mixtures indicates that the crucial carbide-phosphide interaction is established during decomposition (step 3, Scheme 1) rather than annealing (step 4, Scheme 1). Presence of acidic and basic sites on Mo_2C surfaces has been proposed to facilitate the deposition of phosphide on carbides surface by stabilizing reactions intermediates in close proximity so that phosphidation of in-situ formed metal nanoparticles can proceed.[30, 52]

A reduction of 37-52 mV in HER overpotential for CPCs when compared to Mo_2C is remarkable, but it cannot be attributed solely to the substitution of carbide active sites with more efficient active sites from phosphides. Additionally, phosphides deposited on MWCNT also have lower activity than the CPCs. Considering previously reported activity for phosphide electrocatalysts and the catalyst loadings used here, the results indicate positive enhancements in electrocatalytic activities from the interfacial interaction between carbide and phosphide. Comparable ECSA and Tafel slopes for composite catalysts to Mo_2C indicate that the phosphide nanoparticles do not aggregate when supported on carbide. The large overpotential required for P-MW in Table 1 indicates that probable P doping into MWCNT is also not responsible for the observed reduction in HER overpotentials for CPCs.

Overpotentials to reach 10 mA cm^{-2} activity is one of the most widely reported parameters to compare the activities of nanostructured electrocatalysts.[7] However, catalyst loading must also be considered, as is apparent from Figure 4a. An ideal comparison would be to accurately determine the HER active site densities. However, methods to properly identify active sites have not been developed for the majority of the available nanocrystalline electrocatalysts. Thus, comparing activity with respect to catalyst loading on a working electrode provides the most reasonable comparison.

The HER overpotential needed to generate 10 mA cm^{-2} current densities can be lowered from 154 mV to 79 mV when catalyst loading is increased from 0.2-3 mg cm^{-2}. These overpotentials at elevated loadings compare favorably to other non-precious metal based electrocatalysts.[16, 53] Lower overpotentials have been achieved by mostly using self-supported materials as working electrodes, resembling even higher catalyst loading than employed in Figure 4a. However, unlike the composites discussed here, some of the electrode materials also possess very low Tafel slopes, which are perhaps a better reflection of intrinsic catalytic activity of an active site.[8, 54, 55] Future endeavors to prepare rationally designed composites of carbide and phosphide possessing lower Tafel slopes have the potential to drive the overpotentials even lower.

The enhancement in catalytic activity of CPCs compared to Mo_2C, unsupported phosphides, TMP-MW, and physical mixtures can either be attributed to an increase in surface area, and thus the average number of active sites, or to the carbide-phosphide interaction and the presence of new and more active interfacial sites. The low ECSAs and high overpotentials for unsupported phosphides (Table 1) suggest that these agglomerate rapidly during annealing. Agglomeration can be prevented by

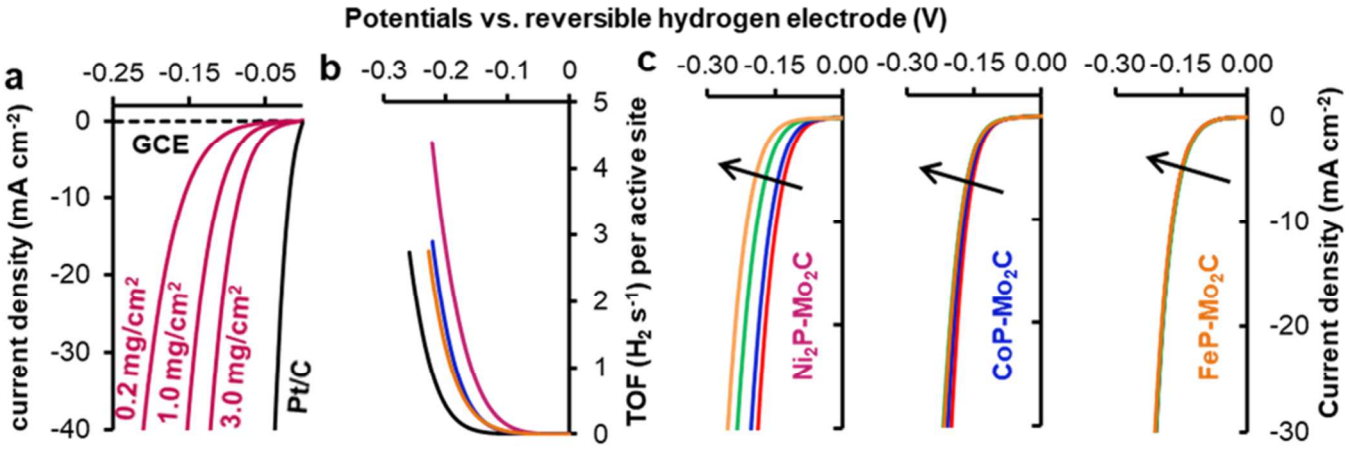

Figure 4. (a) HER polarization curves for Ni_2P-Mo_2C catalyst in 0.5 M H_2SO_4. GCE is bare glassy carbon electrode and Pt/C is 30 weight % Pt on carbon. (b) Turn over frequency (TOF) plots of Mo_2C (black); and FeP (orange), CoP (blue) and Ni_2P (purple) loaded CPCs at 0.2 mg cm^{-2}. (c) HER polarization curves for the composite catalysts collected after 0 hr (red), 6 hr (blue), 12 hour (green), 18 hr (orange) of constant potential electrolysis (CPE) at applied iR corrected potentials corresponding to 10 mA cm^{-2}.

using a high surface area support such as MWCNT; this effect is apparent from the increased ECSA for CPCs, physical mixtures, and TMP-MW. However, while supporting phosphides on MWCNT improves the activity and evidently prevents agglomeration (as is evident from a decrease in overpotential and an increase in ECSA, respectively), the ECSA for TMP-MW are still much lower than those for CPCs and physical mixtures. Presence of carbide in the support matrix leads to increased ECSA, but an increase in ECSA alone does not necessarily lead to a decrease in overpotential or an increase in catalytic activity. In fact, physical mixtures show poorer catalytic activities in comparison to CPCs despite their possessing higher ECSA. Thus, turn over frequency (TOF) was calculated to gain additional insight into the possible interfacial active sites.

In the absence of relevant information to characterize and quantify the nature and density of active sites in nanostructured heterogeneous catalysts, TOF calculations have to be limited to estimation. To determine TOF for electrocatalysts that contain Mo, previous reports have either considered every atom as an active site or considered only metal sites to be HER active.[53, 56] All metal and nonmetal atoms were assumed to be active sites to plot TOF curves in Figure 4b (additional details in the supporting information). As shown in Figure 4b and Table 2, composite catalysts have higher TOF than Mo_2C at all relevant HER overpotentials.

The TOFs for composites are also higher at relevant overpotentials than the other modified Mo_2C catalysts such as S-decorated Mo_2C reported by Tang et al.[56] The actual TOF of composites are likely to be even higher because not all atoms are likely to be active sites. Measured ECSA most probably includes some contribution from carbon that does not necessarily take part in HER at the relevant overpotentials. The enhancements in TOF can also either be attributed to formation of more active carbide-phosphide interfacial sites or active sites from deposited phosphides intrinsically being more efficient than the carbide active sites. The composites have higher activity and TOF at similar loading and overpotentials than previously described unsupported phosphides.[14, 57] Evidently, the carbide-phosphide interaction is providing an enhancement in catalytic activity.

Table 2. TOF (H_2 s^{-1} per active site) at 200 mV overpotentials, change in ECSA and HER overpotentials for 10 mA cm^{-2} activity before and after CPE for 18 hours, and metal concentrations in spent electrolytes (M = Ni/Co/Fe for composites and Mo for Mo_2C).

	Ni2P-Mo2C	CoP-Mo2C	FeP-Mo2C	Mo2C
TOF	2.78	1.61	1.30	0.43
Δη (mV)	65	12	1	-8
ΔECSA (%)	56	19	4	6
[M] (ppm)	0.22	0.14	0.07	0.00

3.4 Electrochemical stability. When the composite catalysts were evaluated using constant potential electrolysis (CPE) to generate 10 mA cm^{-2} current densities, FeP-Mo_2C showed the optimal electrochemical stability followed by CoP-$M_{O_2}C$ (Figure S4). The HER stability trend for the composite catalysts in Figure 4c and summarized in Table 2 parallels the degree of lattice mismatch between phosphide and carbide (Table S4). FeP possesses two sets of planes with extremely low lattice mismatch (<0.2 %) with those in Mo_2C. Similarly, CoP has just one set of lattice planes with extremely low mismatch and shows poorer stability than FeP-Mo_2C, but it is more stable than Ni_2P-Mo_2C. Ni_2P does not have any set of lattice

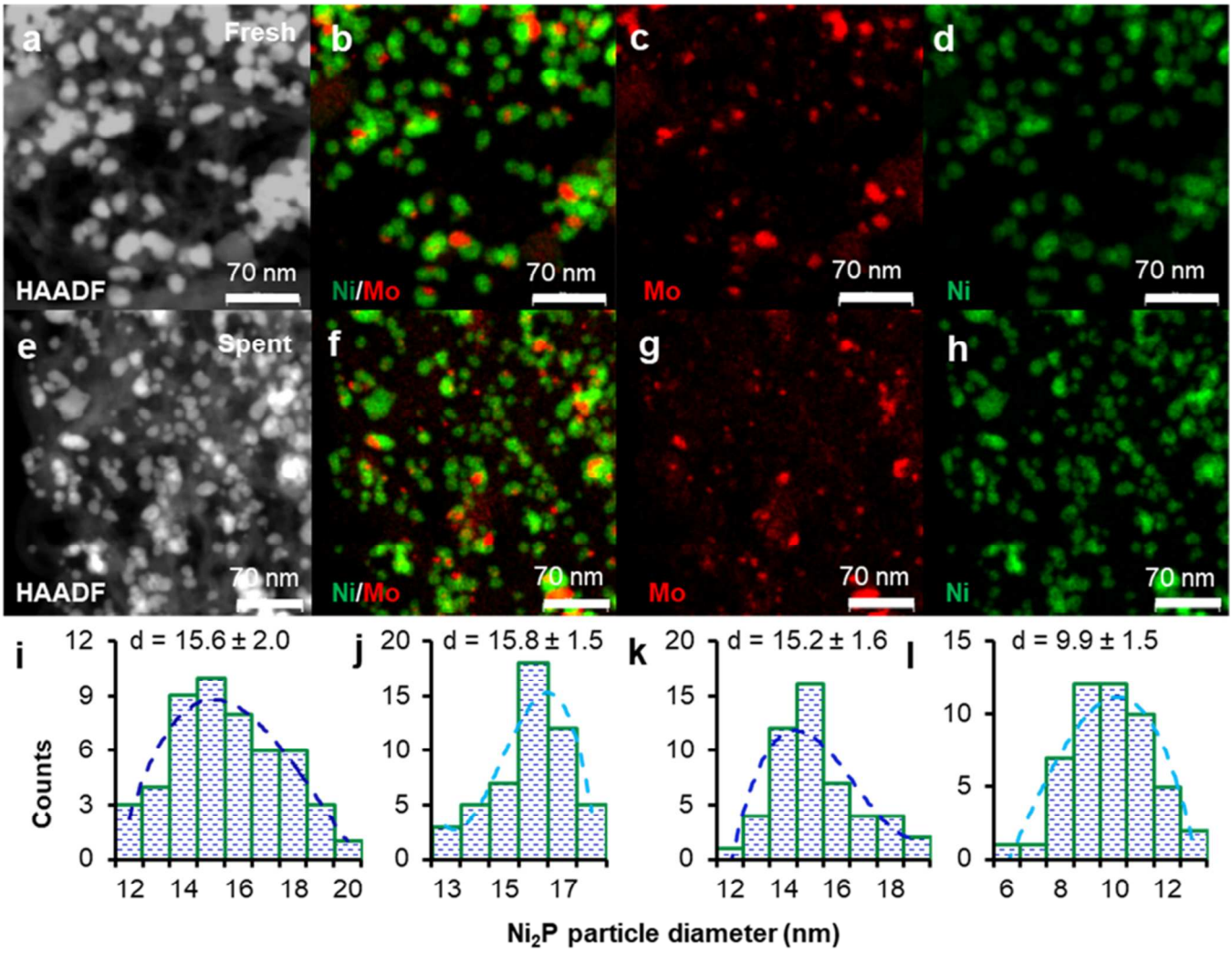

Figure 5. HAADF image and EDS maps of fresh (a-d) and spent (e-h) Ni_2P-Mo_2C. Nickel (green) and molybdenum (red) are overlaid in b and f. Particle size distribution of Ni_2P in the composite catalyst corresponding to i) fresh catalyst with Ni_2P deposited on Mo_2C j) fresh catalyst with Ni_2P not directly deposited on Mo_2C k) spent catalyst with Ni_2P deposited on Mo_2C and l) spent catalyst with Ni_2P not directly deposited on Mo_2C. Direct deposition implies overlap of Mo and Ni in EDS maps.

planes that have lower than 2.2 % mismatch with Mo_2C lattice planes. The trend indicates that carbide-phosphide interaction is responsible for both activity enhancement and electrochemical stability.

The changes in ECSA in Table 2 follow a similar trend, with minimal loss in ECSA over 18 h of CPE for FeP-Mo_2C. The HER activity and ECSA losses in CoP-Mo_2C and Ni_2P-Mo_2C are unlikely due to the degradation of the carbide support, since unadulterated Mo_2C shows minimal loss in ECSA. Mo is also not detected in the electrolyte after 18 hours of our stability test. This indicates that Mo_2C is extremely stable under HER electrocatalysis in acid, as we have previously reported.[27] Post-CPE Mo concentrations, measured using ICP-OES for composites, are also similar to unadulterated Mo_2C.

CPE plots of MP-MW (Figure S5) and HER polarization curves at six hour intervals (Figure S6) further demonstrate the utility of carbide-phosphide interaction in electrochemical stability. While the electrochemical stabilities of CPCs in Figure 4c show a trend paralleling the degree of lattice mismatch all MP-MW degrade significantly under the applied electrochemical conditions in Figure S6.

The activity losses in Table 2 can be attributed to either agglomeration of the nanoparticles during the course of 18 hour CPE or dissolution of catalyst into the electrolyte. Large area EDS maps (Figure S7) before and after CPE tests do not indicate any agglomeration of carbide or phosphide during catalysis. However, ICP-OES measurements for metal ions in the spent electrolyte in Table 2 suggest that at least some of the activity loss is due to phosphide dissolution. Comparison of the Ni_2P-Mo_2C STEM-EDS maps in Figure 5 for fresh (b-d) and spent (f-h) catalysts with corresponding TEM images (Figure S8) reveals that the population of relatively small nickel phosphide particles increases significantly after long-term electrocatalysis. As-prepared phosphide particles (Figure 5d) are significantly more homogeneous than those after catalysis (Figure 5h). The spent catalyst contains a mix-

ture of larger phosphide particles (similar to the fresh catalyst) in addition to much smaller particles.

As shown in Figure 5i-l, the average particle diameter of nickel phosphide associated with carbide in the fresh sample (i) was roughly the same in the spent catalyst (k), whereas the size of unassociated nickel phosphide particles (j) reduced significantly after testing (l). Similar comparison of CoP-Mo2C in Figure S9 for fresh (a-d) and spent (e-h) catalyst shows no apparent size reduction in phosphide particles while tubular geometry of FeP (Figure S10) structures prevents such analysis. Composite EDS maps (Figure S9b and S9f) of CoP-Mo2C for the two transition metals also show better overlap than the corresponding maps for Ni2P-Mo2C (Figure 5b and 5f) with very little CoP unassociated with Mo2C. The lower ECSA and higher Tafel slopes for Ni2P-Mo2C in comparison to other CPCs in Table 1 suggest that higher lattice mismatch between Ni2P and Mo2C leads to phosphide aggregation during annealing. Better overlap of the CoP with carbide in comparison to Ni2P in as synthesized materials further emphasizes the utility of rational design of heterostructures based on lattice mismatch. The FeP crystallites form long tubular structures with smaller particles dispersed throughout. It has previously been observed that incasing FeP in carbon shell prevents dissolution in acid electrolyte.58 While merely supporting FeP on MWCNT cannot prevent the electrochemical degradation (Figure S6c), formation of CPCs also prevent FeP dissolution and shows even longer term stability, as evident from Figure 4c, Figure S4c and Table 2.

4. CONCLUSIONS

In summary, unique carbide-phosphide nanocomposites have been synthesized using a relatively simple and scalable sequential method combining carbothermic reduction and solvothermal decomposition. Carbide-phosphide composites formed via solvothermal decomposition of acac salts of Ni, Fe, and Co in the presence of nanocrystalline Mo2C can be rationally prepared to develop active electrocatalysts. The bimetallic materials evidently contain new active sites as reflected by higher TOF. In conjunction with ICP-OES measurements, we infer that carbide-phosphide interactions prevent dissolution of phosphide particles into the acid electrolyte. Additionally, a low degree of lattice mismatch is responsible for maintaining the carbide-phosphide particles intact, which improves long-term electrochemical stability.

ASSOCIATED CONTENT

Electronic Supplementary Information (ESI) available: XPS survey plots, elemental composition and peak deconvolution data, HRTEM, EDS spectrum, lattice parameters, electrochemistry calculations and CPE plots. This material is available free of charge via the Internet at http://pubs.acs.org.

AUTHOR INFORMATION

Corresponding Author

* (yregmi@utk.edu and schmely@utk.edu

Author Contributions

All authors have given approval to the final version of the manuscript and declare no competing financial interest.

Funding Sources

This project was supported by Southeastern Sun Grant Center and the US Department of Transportation, Research and Innovative Technology Administration DTO559-07-G-00050. N.L and S.C.C. also acknowledge the Southeastern Partnership for Integrated Biomass Supply Systems (IBSS), which is supported by AFRI 2011-68005-30410 from USDA NIFA. XRD was performed at the Joint Institute for Advanced Materials (JIAM) by using instruments that were procured through the DOE Nuclear Energy University Program (DE-NE0000693) 12–3528. STEM, EELS and XPS were performed at the Materials Science and Technology Division, Oak Ridge National Laboratory.

ACKNOWLEDGMENT

The authors would like to thank Ms. Choo Hamilton at the Center for Renewable Carbon (CRC) for assistance with ICP-OES and Dr. Brian T. Sneed at the Center for Nanophase Materials Sciences, Oak Ridge National Laboratory for help with visualization softwares.

REFERENCES

(1) Hunter, B. M.; Gray, H. B.; Muller, A. M., Earth-Abundant Heterogeneous Water Oxidation Catalysts. *Chem. Rev.* **2016,** 116, (22), 14120-14136.

(2) Zheng, Y.; Jiao, Y.; Jaroniec, M.; Qiao, S. Z., Advancing the electrochemistry of the hydrogen-evolution reaction through combining experiment and theory. *Angew. Chem. Int. Ed. Engl.* **2015,** 54, (1), 52-65.

(3) Zou, X.; Zhang, Y., Noble metal-free hydrogen evolution catalysts for water splitting. *Chem. Soc. Rev.* **2015,** 44, (15), 5148-5180.

(4) Faber, M. S.; Jin, S., Earth-abundant inorganic electrocatalysts and their nanostructures for energy conversion applications. *Energy Environ. Sci.* **2014,** 7, (11), 3519-3542.

(5) Safizadeh, F.; Ghali, E.; Houlachi, G., Electrocatalysis developments for hydrogen evolution reaction in alkaline solutions – A Review. *Int. J. Hyd. Energ.* **2015,** 40, (1), 256-274.

(6) Winther-Jensen, B.; MacFarlane, D. R., New generation, metal-free electrocatalysts for fuel cells, solar cells and water splitting. *Energy Environ. Sci.* **2011,** 4, (8), 2790-2798.

(7) McCrory, C. C.; Jung, S.; Ferrer, I. M.; Chatman, S. M.; Peters, J. C.; Jaramillo, T. F., Benchmarking hydrogen evolving reaction and oxygen evolving reaction electrocatalysts for solar water splitting devices. *J. Am. Chem. Soc.* **2015,** 137, (13), 4347-57.

(8) Benck, J. D.; Hellstern, T. R.; Kibsgaard, J.; Chakthranont, P.; Jaramillo, T. F., Catalyzing the Hydrogen Evolution Reaction (HER) with Molybdenum Sulfide Nanomaterials. *ACS Catal.* **2014,** 4, (11), 3957-3971.

(9) Chen, W. F.; Wang, C. H.; Sasaki, K.; Marinkovic, N.; Xu, W.; Muckerman, J. T.; Zhu, Y.; Adzic, R. R., Highly active and durable nanostructured molybdenum carbide electrocatalysts for hydrogen production. *Energy Environ. Sci.* **2013,** 6, (3), 943-951.

(10) Wu, H. B.; Xia, B. Y.; Yu, L.; Yu, X. Y.; Lou, X. W., Porous molybdenum carbide nano-octahedrons synthesized via confined carburization in metal-organic frameworks for efficient hydrogen production. *Nat. Commun.* **2015,** 6, 6512.

(11) Zhong, Y.; Xia, X.; Shi, F.; Zhan, J.; Tu, J.; Fan, H. J., Transition Metal Carbides and Nitrides in Energy Storage and Conversion. *Adv. Sci. (Weinh)* **2016,** 3, (5), 1500286.

(12) Lee, J. S., Oyama, S. T., Boudart, M., Molybdenum carbide catalysts I. Synthesis of unsupported powders. *J. Catal.* **1987,** 106, (1), 125-133.

(13) Regmi, Y. N.; Wan, C.; Duffee, K. D.; Leonard, B. M., Nanocrystalline Mo2C as a Bifunctional Water Splitting Electrocatalyst. *ChemCatChem* **2015,** 7, (23), 3911-3915.

(14) Xiao, P.; Chen, W.; Wang, X., A Review of Phosphide-Based Materials for Electrocatalytic Hydrogen Evolution. *Adv. Energy Mater.* **2015,** 5, (24), 1500985.

(15) Sun, M.; Liu, H.; Qu, J.; Li, J., Earth-Rich Transition Metal Phosphide for Energy Conversion and Storage. *Adv. Energy Mater.* **2016,** 6, (13), 1600087.

(16) Callejas, J. F.; Read, C. G.; Roske, C. W.; Lewis, N. S.; Schaak, R. E., Synthesis, Characterization, and Properties of Metal Phosphide Catalysts for the Hydrogen-Evolution Reaction. *Chem. Mater.* **2016,** 28, (17), 6017-6044.

(17) Han, A.; Jin, S.; Chen, H.; Ji, H.; Sun, Z.; Du, P., A robust hydrogen evolution catalyst based on crystalline nickel phosphide nanoflakes on three-dimensional graphene/nickel foam: high performance for electrocatalytic hydrogen production from pH 0–14. *J. Mater. Chem. A* **2015,** 3, (5), 1941-1946.

(18) Popczun, E. J.; McKone, J. R.; Read, C. G.; Biacchi, A. J.; Wiltrout, A. M.; Lewis, N. S.; Schaak, R. E., Nanostructured nickel phosphide as an electrocatalyst for the hydrogen evolution reaction. *J. Am. Chem. Soc.* **2013,** 135, (25), 9267-70.

(19) Gu, S.; Du, H.; Asiri, A. M.; Sun, X.; Li, C. M., Three-dimensional interconnected network of nanoporous CoP nanowires as an efficient hydrogen evolution cathode. *Phys. Chem. Chem. Phys.* **2014,** 16, (32), 16909-16913.

(20) Bai, Y.; Zhang, H.; Li, X.; Liu, L.; Xu, H.; Qiu, H.; Wang, Y., Novel peapod-like Ni(2)P nanoparticles with improved electrochemical properties for hydrogen evolution and lithium storage. *Nanoscale* **2015,** 7, (4), 1446-1453.

(21) Ma, B.; Xu, H.; Lin, K.; Li, J.; Zhan, H.; Liu, W.; Li, C., Mo2 C as Non-Noble Metal Co-Catalyst in Mo2 C/CdS Composite for Enhanced Photocatalytic H2 Evolution under Visible Light Irradiation. *ChemSusChem* **2016,** 9, (8), 820-824.

(22) Ma, B.; Liu, Y.; Li, J.; Lin, K.; Liu, W.; Zhan, H., Mo2N: An efficient non-noble metal cocatalyst on CdS for enhanced photocatalytic H2 evolution under visible light irradiation. *Int. J. Hyd. Energ.* **2016,** 41, (47), 22009-22016.

(23) Ma, B.; Wang, X.; Lin, K.; Li, J.; Liu, Y.; Zhan, H.; Liu, W., A novel ultraefficient non-noble metal composite cocatalyst Mo 2 N/Mo 2 C/graphene for enhanced photocatalytic H 2 evolution. *Int. J. Hyd. Energ.* **2017,** 42, (30), 18977-18984.

(24) Nellist, M. R.; Laskowski, F. A.; Lin, F.; Mills, T. J.; Boettcher, S. W., Semiconductor-Electrocatalyst Interfaces: Theory, Experiment, and Applications in Photoelectrochemical Water Splitting. *Acc. Chem. Res.* **2016,** 49, (4), 733-740.

(25) Fabian, D. M.; Hu, S.; Singh, N.; Houle, F. A.; Hisatomi, T.; Domen, K.; Osterloh, F. E.; Ardo, S., Particle suspension reactors and materials for solar-driven water splitting. *Energy Environ. Sci.* **2015,** 8, (10), 2825-2850.

(26) Haussener, S.; Xiang, C.; Spurgeon, J. M.; Ardo, S.; Lewis, N. S.; Weber, A. Z., Modeling, simulation, and design criteria for photoelectrochemical water-splitting systems. *Energy Environ. Sci.* **2012,** 5, (12), 9922-9935.

(27) Hu, S.; Xiang, C.; Haussener, S.; Berger, A. D.; Lewis, N. S., An analysis of the optimal band gaps of light absorbers in integrated tandem photoelectrochemical water-splitting systems. *Energy Environ. Sci.* **2013,** 6, (10), 2984-2993.

(28) Kudo, A.; Miseki, Y., Heterogeneous photocatalyst materials for water splitting. *Chem. Soc. Rev.* **2009,** 38, (1), 253-78.

(29) Regmi, Y. N.; Roy, A.; Goenaga, G. A.; McBride, J. R.; Rogers, B. R.; Zawodzinski, T. A.; Labbé, N.; Chmely, S. C., Electrocatalytic Activity and Stability Enhancement through Preferential Deposition of Phosphide on Carbide. *ChemCatChem* **2017,** 9, (6), 1054-1061.

(30) Regmi, Y. N.; Rogers, B. R.; Labbé, N.; Chmely, S. C., Scalable and Tunable Carbide–Phosphide Composite Catalyst System for the Thermochemical Conversion of Biomass. *ACS Sustainable Chem. Eng.,* **2017**, 5 (9), pp 7751–7758.

(31) Wang, J.; Johnston-Peck, A. C.; Tracy, J. B., Nickel Phosphide Nanoparticles with Hollow, Solid, and Amorphous Structures. *Chem. Mater.* **2009,** 21, (19), 4462-4467.

(32) She, H.; Chen, Y.; Wen, R.; Zhang, K.; Yue, G. H.; Peng, D. L., A nonaqueous approach to the preparation of iron phosphide nanowires. *Nanoscale Res. Lett.* **2010,** 5, (4), 786-790.

(33) Li, Y.; Malik, M. A.; O'Brien, P., Synthesis of single-crystalline CoP nanowires by a one-pot metal-organic route. *J. Am. Chem. Soc.* **2005,** 127, (46), 16020-16021.

(34) Regmi, Y. N.; Leonard, B. M., General Synthesis Method for Bimetallic Carbides of Group VIIIA First Row Transition Metals with Molybdenum and Tungsten. *Chem. Mater.* **2014,** 26, (8), 2609-2616.

(35) Callejas, J. F.; Read, C. G.; Popczun, E. J.; McEnaney, J. M.; Schaak, R. E., Nanostructured Co2P Electrocatalyst for the Hydrogen Evolution Reaction and Direct Comparison with Morphologically Equivalent CoP. *Chem. Mater.* **2015,** 27, (10), 3769-3774.

(36) Kawasaki, S.; Matsuoka, Y.; Yokomae, T.; Nojima, Y.; Okino, F.; Touhara, H.; Kataura, H., XRD and TEM study of high pressure treated single-walled carbon nanotubes and C60-peapods. *Carbon* **2005,** 43, (1), 37-45.

(37) Tian, J.; Liu, Q.; Asiri, A. M.; Sun, X., Self-supported nanoporous cobalt phosphide nanowire arrays: an efficient 3D hydrogen-evolving cathode over the wide range of pH 0-14. *J. Am. Chem. Soc.,* **2014,** 136, (21), 7587-7590.

(38) Liang, Y.; Liu, Q.; Asiri, A. M.; Sun, X.; Luo, Y., Self-Supported FeP Nanorod Arrays: A Cost-Effective 3D Hydrogen Evolution Cathode with High Catalytic Activity. *ACS Catal.* **2014,** 4, (11), 4065-4069.

(39) Wang, X.; Kolen'ko, Y. V.; Bao, X. Q.; Kovnir, K.; Liu, L., One-Step Synthesis of Self-Supported Nickel Phosphide Nanosheet Array Cathodes for Efficient Electrocatalytic Hydrogen Generation. *Angew. Chem. Int. Ed. Engl.* **2015,** 54, (28), 8188-8192.

(40) Wan, C.; Leonard, B. M., Iron-Doped Molybdenum Carbide Catalyst with High Activity and Stability for the Hydrogen Evolution Reaction. *Chem. Mater.* **2015,** 27, (12), 4281-4288.

(41) Lin, H.; Liu, N.; Shi, Z.; Guo, Y.; Tang, Y.; Gao, Q., Cobalt-Doping in Molybdenum-Carbide Nanowires Toward Efficient Electrocatalytic Hydrogen Evolution. *Adv. Funct. Mater.* **2016,** 26, (31), 5590-5598.

(42) Xu, X.; Nosheen, F.; Wang, X., Ni-Decorated Molybdenum Carbide Hollow Structure Derived from Carbon-Coated Metal–Organic Framework for Electrocatalytic Hydrogen Evolution Reaction. *Chem. Mater.* **2016,** 28, (17), 6313-6320.

(43) Franke, R.; Chassé, T.; Streubel, P.; Meisel, A., Auger parameters and relaxation energies of phosphorus in solid compounds. *J. Electron. Spectrosc. Relat. Phenom.* **1991,** 56, (4), 381-388.

(44) Myers, C. E.; Franzen, H. F.; Anderegg, J. W., X-ray photoelectron spectra and bonding in transition-metal phosphides. *Inorg. Chem.* **1985,** 24, (12), 1822-1824.

(45) Haber, J.; Ungier, L., On chemical shifts of ESCA and Auger lines in cobalt oxides. *J. Electron. Spectrosc. Relat. Phenom.* **1977,** 12, (3), 305-312.

(46) Park, S.-J.; Jang, Y.-S., X-ray diffraction and X-ray photoelectron spectroscopy studies of Ni–P deposited onto carbon fiber surfaces: impact properties of a carbon-fiber-reinforced matrix. *J. Colloid Interface Sci.* **2003,** 263, (1), 170-176.

(47) Henderson, L. B.; Ekerdt, J. G., Effect of Phosphorus and Carbon Incorporation in Amorphous Cobalt Films Prepared by Chemical Vapor Deposition. *J. Electrochem. Soc.* **2010,** 157, (1), D29.

(48) Zhangping, S.; Nie, K.; Shao, Z.; Gao, B.; Lin, H.; Zhang, H.; Liu, B.; Wang, Y.; Zhang, Y.; Sun, X.; Cao, X.; Hu, P.; Gao, Q.; Tang, Y., Phosphorus-Mo2C@Carbon Nanowires toward Efficient Electrochemical Hydrogen Evolution: Composition, Structural and Electronic Regulation. *Energy Environ. Sci.* **2017,** 10,(5), 1262-1271.

(49) McEnaney, J. M.; Crompton, J. C.; Callejas, J. F.; Popczun, E. J.; Biacchi, A. J.; Lewis, N. S.; Schaak, R. E., Amorphous Molybdenum Phosphide Nanoparticles for Electrocatalytic Hydrogen Evolution. *Chem. Mater.* **2014,** 26, (16), 4826-4831.

(50) McCrory, C. C.; Jung, S.; Peters, J. C.; Jaramillo, T. F., Benchmarking heterogeneous electrocatalysts for the oxygen evolution reaction. *J. Am. Chem. Soc.* **2013,** 135, (45), 16977-87.

(51) Jung, S.; McCrory, C. C. L.; Ferrer, I. M.; Peters, J. C.; Jaramillo, T. F., Benchmarking nanoparticulate metal oxide electrocatalysts for the alkaline water oxidation reaction. *J. Mater. Chem. A* **2016,** 4, (8), 3068-3076.

(52) Baddour, F. G.; Nash, C. P.; Schaidle, J. A.; Ruddy, D. A., Synthesis of alpha-MoC1-x Nanoparticles with a Surface-Modified SBA-15 Hard Template: Determination of Structure-Function Relationships in Acetic Acid Deoxygenation. *Angew. Chem. Int. Ed. Engl.* **2016,** 55, (31), 9026-9029.

(53) Kibsgaard, J.; Jaramillo, T. F., Molybdenum phosphosulfide: an active, acid-stable, earth-abundant catalyst for the hydrogen evolution reaction. *Angew. Chem. Int. Ed. Engl.* **2014,** 53, (52), 14433-14437.

(54) Laursen, A. B.; Patraju, K. R.; Whitaker, M. J.; Retuerto, M.; Sarkar, T.; Yao, N.; Ramanujachary, K. V.; Greenblatt, M.; Dismukes, G. C., Nanocrystalline Ni5P4: a hydrogen evolution electrocatalyst of exceptional efficiency in both alkaline and acidic media. *Energy Environ. Sci.* **2015,** 8, (3), 1027-1034.

(55) Xia, C.; Liang, H.; Zhu, J.; Schwingenschlögl, U.; Alshareef, H. N., Active Edge Sites Engineering in Nickel Cobalt Selenide Solid Solutions for Highly Efficient Hydrogen Evolution. *Adv. Energy Mater.* **2017,** 1602089.

(56) Tang, C.; Wang, W.; Sun, A.; Qi, C.; Zhang, D.; Wu, Z.; Wang, D., Sulfur-Decorated Molybdenum Carbide Catalysts for Enhanced Hydrogen Evolution. *ACS Catal.* **2015,** 5, (11), 6956-6963.

(57) Seo, B.; Baek, D. S.; Sa, Y. J.; Joo, S. H., Shape effects of nickel phosphide nanocrystals on hydrogen evolution reaction. *CrystEngComm* **2016,** 18, (32), 6083-6089.

(58) Chung, D. Y.; Jun, S. W.; Yoon, G.; Kim, H.; Yoo, J. M.; Lee, K. S.; Kim, T.; Shin, H.; Sinha, A. K.; Kwon, S. G.; Kang, K.; Hyeon, T.; Sung, Y. E., Large-Scale Synthesis of Carbon-Shell-Coated FeP Nanoparticles for Robust Hydrogen Evolution Reaction Electrocatalyst. *J. Am. Chem. Soc.* ***2017****, 139 (19), 6669–6674*.

Table of content

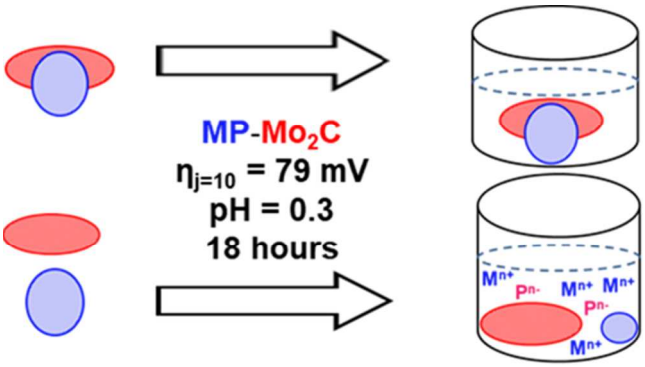

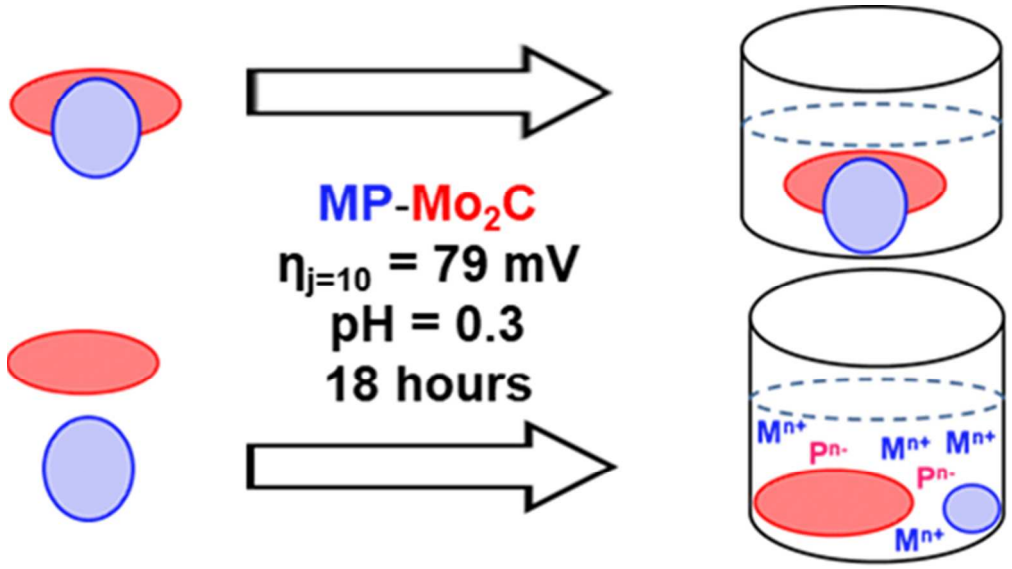

84x47mm (300 x 300 DPI)